ChemComm

COMMUNICATION

View Article Online
View Journal | View Issue

Cite this: *Chem. Commun.*, 2023, 59, 6255

Received 6th March 2023,
Accepted 19th April 2023

DOI: 10.1039/d3cc01100c

rsc.li/chemcomm

Hexachlorotriphosphazene-assisted buried interface passivation for stable and efficient wide-bandgap perovskite solar cells†

Ruyue Wang,‡ Minghua Li,‡ Zongwen Ma, Zhangwei He, Yiman Dong, Yuling Zhang, Zhiyang Xu, Gangfeng Su and Zhan'ao Tan *

Large open-circuit voltage (V_{oc}) loss is the main issue limiting the efficiency improvement in wide bandgap perovskite solar cells (PerSCs). Herein, a facile buried interface treatment by hexachlorotriphosphazene is developed to suppress the V_{oc} loss. The PerSCs include a $[Cs_{0.22}FA_{0.78}Pb(I_{0.85}Br_{0.15})_3]_{0.97}(MAPbCl_3)_{0.03}$ (1.67 eV) absorber and deliver an efficiency of 21.47% and a V_{oc} of 1.21 V (V_{oc} loss of 0.46 V). More importantly, the unencapsulated PerSCs maintain 90% of the initial efficiency after aging 500 h in N_2.

Recently, perovskite solar cells (PerSCs) have achieved extraordinary progress with a rapid power conversion efficiency (PCE) increase from 3.8% to 25.7%, approaching the Shockley–Queisser (S–Q) limit in single-junction solar cells.[1,2] In order to surpass the S–Q limit, two terminal (2T) or four terminal (4T) tandem devices were designed. The theoretical efficiencies of 2T and 4T tandem configurations can be over 46%, remarkably higher than the ~33% efficiency for a single junction cell under 1 sun illumination.[3,4] This is because the wide bandgap (WBG) top cell and narrow bandgap (NBG) bottom cell complementarily absorb the light, which can significantly improve the light energy utilization and reduce the thermal loss of charge carriers, and thereby achieve further improvement in the PCE.[5–8] For tandem solar cells (TSCs), WBG PerSCs play a more essential role in harvesting high-energy photons and providing a high open-circuit voltage (V_{oc}).[9]

WBG PerSCs are usually composed of a high content of Cs ions at the A sites or a high content of bromine ions at the X sites to regulate the perovskite bandgap with over 1.65 eV.[10] The performance of WBG PerSCs has been limited by the V_{oc} deficit due to the severe interface recombination loss, which originates from film defects or energy level mismatch between the perovskite layer and the charge transport layer. To solve this, many methods have been used to improve the film quality of WBG perovskites, such as composition optimization, additive coordination, solvent engineering and defect passivation.[11–14] However, the processing complexity and low reproducibility restrain a wide application. A more efficient strategy is urgently needed to further mitigate V_{oc} deficits in WBG PerSCs to accelerate the development of perovskite-based TSCs.[15,16]

In this work, hexachlorotriphosphazene (HCCP) is employed to optimize the interface quality between the perovskite and underlying hole transport layer in p–i–n WBG PerSCs. The HCCP effectively improves the wettability of the hole transport layer poly[bis(4-phenyl) (2,4,6-trimethylphenyl) amine] (PTAA), reduces the trap-assisted non-radiative recombination and improves V_{oc}. Consequently, HCCP-treated WBG PerSCs with a 1.67 eV bandgap perovskite absorber layer demonstrate a high efficiency of 21.74% with a small V_{oc} deficit of 0.46 V, which is one of the best reported in WBG PerSCs. Moreover, the unencapsulated PerSCs show an improved stability by maintaining 90% of the initial efficiency after 500 h of storage in N_2 conditions.

Polyphosphazene (HCCP, Fig. 1a) is a representative organic-inorganic hybrid material and exhibits many advantages, such as a simple synthesis, easy purification and low cost.[17] The strong π–π interaction between P and N in the main chain contributes to a favorable structural stability.[18] In the Nuclear Magnetic resonance (NMR) measurement (Fig. 1b and Fig. S1, ESI†), the characteristic ^{31}P peaks of HCCP in the PbI_2-HCCP composite show an obvious shift to a higher δ value compared with that of pure HCCP. The shift of ^{31}P indicates the interaction between P and Pb, leading to a weakened shielding effect because the valence electron deviates from the proton and appears as a signal peak in the low field. In Fig. S2 (ESI†) of a HCCP FTIR, the peaks at 603.24 and 522.83 cm^{-1} are characteristic peaks of P–Cl bonds. The infrared spectrum of the perovskite film (Fig. S3, ESI†) shows that the characteristic peaks of 603.24 and 522.83 cm^{-1} disappear with PbI_2 introduction and the peaks

Beijing Advanced Innovation Center for Soft Matter Science and Engineering, Beijing University of Chemical Technology, Beijing 100029, China.
E-mail: tanzhanao@mail.buct.edu.cn

† Electronic supplementary information (ESI) available. See DOI: https://doi.org/10.1039/d3cc01100c

‡ Ruyue Wang and Dr. Minghua Li contributed equally to this work.

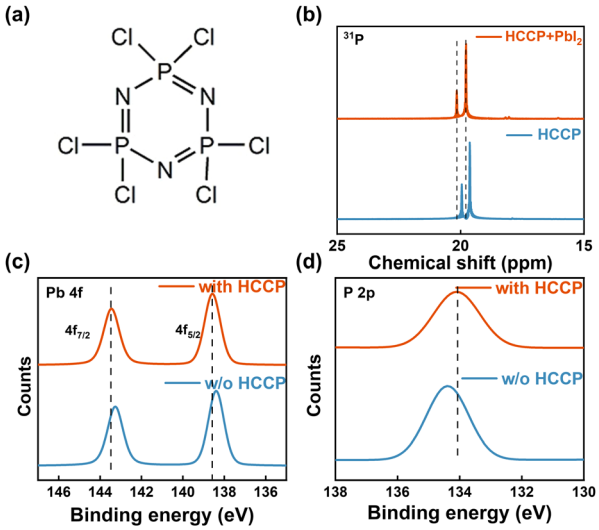

Fig. 1 (a) Structure of HCCP. (b) ^{31}P NMR of HCCP with and without PbI_2. The XPS spectra Pb 4f (c) and P 2p (d) of perovskite films with and without HCCP.

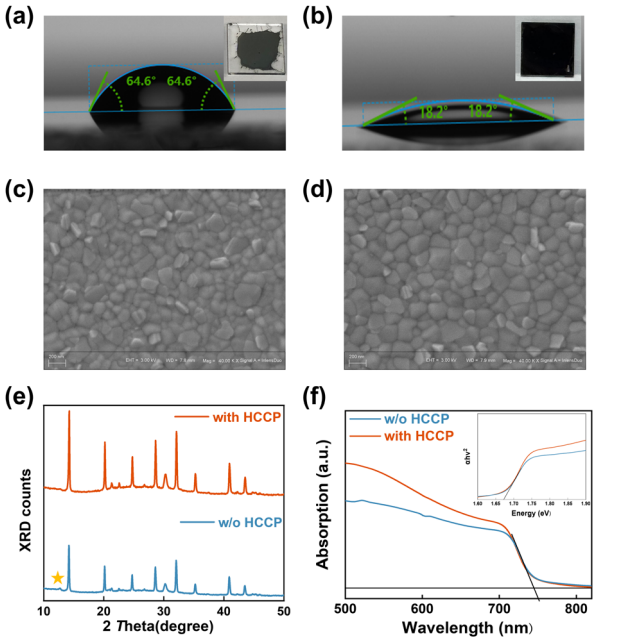

Fig. 2 Surface contact angles of (a) PTAA and (b) PTAA/HC CP. SEM images of the perovskite on (c) PTAA control film and (d) PTAA/HCCP. (e) XRD and (f) UV-vis absorption of perovskite films (Illustrated as a Tauc diagram).

located at 2922.70 and 2853 cm^{-1} shift to 2972.69 and 2826.94 cm^{-1}, respectively, which is evidence confirming the coordination between P and Pb. To better understand the interactions at the interfaces between the perovskite and the HCCP layer, the bonding interactions between perovskite and HCCP are studied by X-ray photoelectron spectroscopy (XPS) measurements (Fig. 1c, d and Fig. S4, ESI†). The Pb 4f peaks shift toward a higher binding energy while the P 2p peak from HCCP shifts toward a lower binding energy. The results confirm the strong interaction bonds between P and Pb.[19,20]

Analysis of the contact property between perovskite and the PTAA or PTAA/HCCP substrates (measured in air) was further conducted (Fig. 2a and b). After stabilization, the contact angles were 64.6° for PTAA and 18.2° for the PTAA/HCCP substrate. This indicates that the HCCP transforms the hydrophobic PTAA surface into a hydrophilic surface, which is beneficial for facilitating the perovskite film deposition (as shown in the insets of Fig. 2a and b). To understand the improvement of a perovskite film by HCCP treatment, scanning electron microscopy (SEM) was utilized to investigate the morphology of perovskite films. There are some obvious protrusions on the surface of the PTAA sample (Fig. 2c), which are usually attributed to the residual excess PbI_2 on the surface of the perovskite film.[21,22] In contrast, the perovskite on PTAA/HCCP presents a uniform and dense morphology (Fig. 2d). As shown in the AFM images (Fig. S5, ESI†), the PTAA/HCCP sample shows a reduced root-mean-square roughness (R_q) of 15.3 nm from 17.0 nm for the PTAA sample. In the X-ray diffraction (XRD) spectrum (Fig. 2e), the two samples show similar peak positions, which indicates that the lattice structure of perovskite is not obviously affected by HCCP incorporation. The diffraction intensity of the (1 1 0) peak is about 1.56 times that of the control sample (Fig. S6, ESI†). According to our basic knowledge of crystallography, this increased diffraction intensity indicates an improved crystallization, which would be related to fewer defects or a more oriented lattice plane. In addition, the PbI_2 peak located at 12.6° disappears in the perovskite film with HCCP treatment, which is more significant for obtaining a high PCE because residual PbI_2 serves as severe recombination centers that lower the carrier transfer efficiency. From these two aspects, we can infer that HCCP treatment is beneficial for improving the crystallization of a perovskite film. UV-vis spectroscopy was used to examine the light-absorbing ability of perovskite films, as shown in Fig. 2f. Due to the reduction of defects leading to a better crystallization of the perovskite, the HCCP modified layer significantly improves the light absorption ability of the perovskite film in the wavelength range of 500 to 700 nm. It is easy to obtain a higher photocurrent in the device preparation. The absorption edge of the two perovskite films is 744 nm according to the UV-vis absorption spectrum. Therefore, we can confirm that the bandgap of the original perovskite and perovskite with HCCP are all 1.67 eV.[23]

Steady-state and time-resolved photoluminescence (PL) measurements were further carried out to investigate the defect passivation effect of HCCP. Compared with the control sample (Fig. 3a), the perovskite film on HCCP shows a stronger emission intensity. Research has shown that deep-level defects in perovskite materials can form nonradiative composite centers, reducing the carrier concentration in the material and leading to a significant decrease in PL.[24] The coordination between HCCP and Pb in perovskite reduces the defects and inhibits non radiative recombination, resulting in an enhanced PL strength. TRPL testing was conducted and fitted using a dual exponential decay function to generate rapid decay (τ_1) and slow decay (τ_2) components (Fig. 3b and Table S1, ESI†).

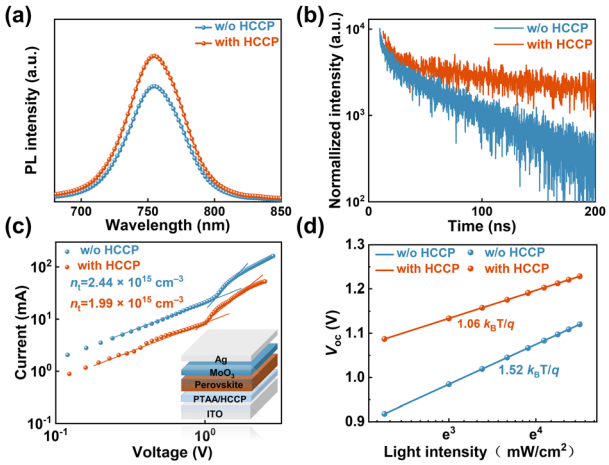

Fig. 3 (a) Steady-state and (b) time-resolved PL spectra. (c) Dark *I*–*V* curves of the hole-only device (Illustrated as a single-hole device structure) (d) Light intensity-dependent open-circuit voltage measurements.

The rapidly decaying component is the carrier capture caused by surface defects in perovskite films, while the slowly decaying component reflects the carrier lifetime limited by body defects in perovskite films.[25,26] For the control sample, the values of τ_1 and τ_2 are 4.83 and 57.67 ns (Table S1, ESI†). With HCCP treatment, the values increase to 6.85 ns and 226.23 ns. The perovskite film with HCCP treatment exhibits an increased carrier lifetime of 185.50 ns from the 39.70 ns of the control film, indicating an effective suppression of non-radiative recombination caused by defects. To clearly recognize the reduced trap density of the perovskite film with HCCP, hole-only devices with the structure of ITO/PTAA (HCCP)/Perovskite/MoO_3/Ag were fabricated. Fig. 3c is obtained by logarithmically processing the voltage and current obtained from the test. The voltage at the point where the current rises rapidly is defined as the trap-filled limit voltage (V_{TFL}) and the trap density can be calculated according to the following equation:

$$V_{TFL} = \frac{en_tL^2}{2\varepsilon\varepsilon_0}$$

where ε is the relative dielectric constant of the perovskite, ε_0 is the vacuum permittivity, e is the elementary electronic charge, L is the film thickness, and n_t is the trap density.[27] The device with HCCP treatment shows a lower V_{TFL} (0.96 V). The calculated hole trap densities (1.99×10^{15} cm^{-3}) for the perovskite film with HCCP treatment are lower than that of the control film (2.44×10^{15} cm^{-3}), which indicates that the HCCP could remarkably decrease the defect density to suppress the non-radiative recombination loss and enhance the device performance. The relationship between V_{oc} and light intensity is further measured (Fig. 3d) to investigate the carrier recombination kinetics of PerSCs under working conditions. The relationship between V_{oc} and light intensity can be expressed by the following equation:

$$V_{oc} = (K_BT/q)\ln(I) + \text{constant}$$

where K_B is the Boltzmann constant, T is the temperature, and q is the elementary charge.[28] The PerSCs with PTAA/HCCP show a reduced slope of 1.06 K_BT/q compared with 1.52 K_BT/q for the control device. This indicates that the introduction of HCCP can effectively inhibit the energy loss caused by trap-assisted recombination. The dependence of J_{sc} on the light intensity is shown in Fig. S7 (ESI†). The slope was 0.99 for the HCCP-treated perovskite device, which was greater than that of 0.97 for the control device, suggesting a better charge transfer performance with a suppressive bimolecular recombination.

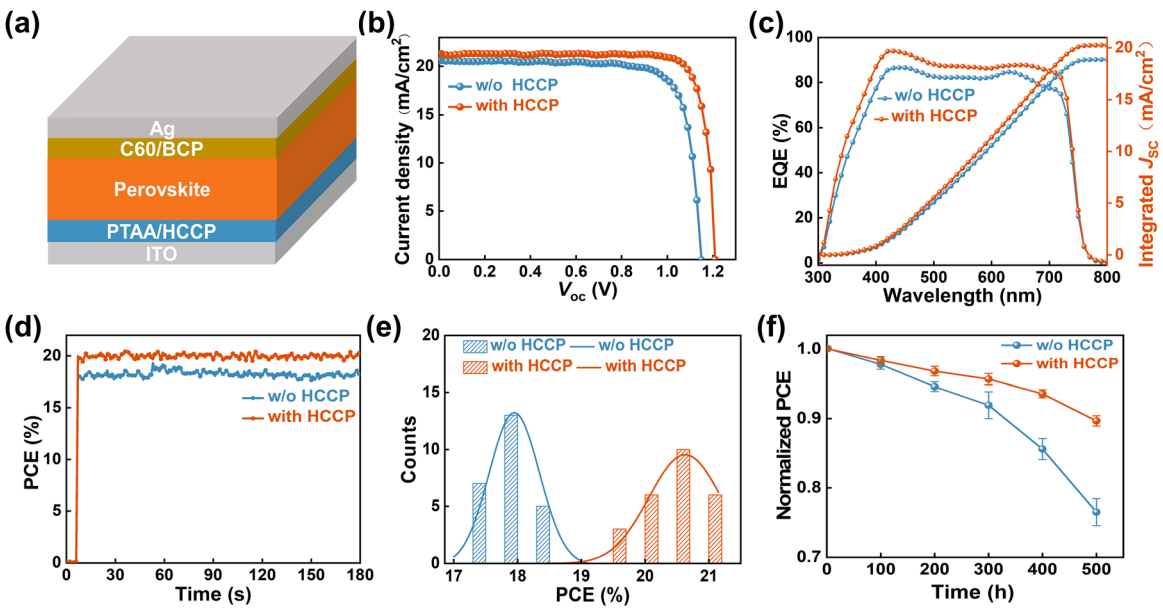

Fig. 4 (a) Schematic diagram of the device structure. (b) *J*–*V* curve of the champion devices with pristine perovskite films and that with HCCP modification. (c) EQE spectra and the consistent integrated current density of the pristine devices and the devices with HCCP modification. (d) Steady-state PCE at the maximum power point. (e) Distribution of PCEs for 25 devices. (f) Device storage stability in a nitrogen-filled glovebox.

To study the HCCP effect on device performance, planar p–i–n PerSCs with the structure ITO/PTAA/Perovskite/C60/BCP/Ag (Fig. 4a) were fabricated. The WBG perovskite with a composition of $[Cs_{0.22}FA_{0.78}Pb(I_{0.85}Br_{0.15})_3]_{0.97}(MAPbCl_3)_{0.03}$ is deposited by a solvent method and delivers a bandgap of 1.67 eV. The *J–V* curves of the champion control and HCCP-treated PerSCs are presented in Fig. 4b and summarized in Table S2 (ESI†). The best HCCP-treated devices achieve an improved PCE of 21.47% with a high V_{oc} of 1.21 V, which is among the best reported among the state-of-the-art WBG PerSCs (Table S3, ESI†). By optimizing the HCCP concentration, the 0.5 mg mL^{-1} condition shows the highest PCE (Fig. S8, ESI†). The external quantum efficiency (EQE) spectrum of the champion PerSCs was measured (Fig. 4c). The integrated J_{sc} values are 18.87 and 20.29 mA cm^{-2}, which are consistent with the values from the *J–V* measurements. The steady-state efficiencies corresponding to the maximum power point of the control and HCCP-treated PerSCs (Fig. 4d) are 18.15% and 21.02%, respectively. The statistical PCE distribution of 25 devices are depicted in Fig. 4e. The HCCP-treated PerSC shows an improved average PCE of 15% compared with 18% of the control device, showing the favorable reliability and repeatability of the HCCP treatment. In addition, the long-term storage stability of PerSCs was studied (Fig. 4f). After 500 hours of storage in a glove box filled with N_2, the unencapsulated device containing HCCP kept 90% of the initial efficiency, while the reference device without HCCP only kept 76% of the initial efficiency.

In conclusion, an effective interface was established for WBG PerSCs by utilizing HCCP between the perovskite and underlying HTL. The HCCP contributes to reduce trap densities in perovskite thin-films and suppresses nonradiative recombination, which is beneficial for an improved FF and V_{oc}. With HCCP treatment, the champion PerSCs deliver an extremely high PCE of 21.47% with a small V_{oc} loss of 0.46 V. In terms of stability, the efficiencies of devices without HCCP rapidly drop to 76% of the initial efficiency after aging in a nitrogen atmosphere for 500 h. In contrast, the HCCP-treated PerSCs show an improved stability by maintaining 90% of the initial PCE. This work provides a new avenue for the preparation of highly efficient and stable WBG PerSCs.

The authors would like to thank the National Natural Science Foundation of China (51873007, 21835006) for the financial support.

Conflicts of interest

There are no conflicts to declare.

Notes and references

1 A. Kojima, K. Teshima, Y. Shirai and T. Miyasaka, *J. Am. Chem. Soc.*, 2009, **131**, 6050.
2 J. Park, J. Kim, H. S. Yun, M. J. Paik, E. Noh, H. J. Mun, M. G. Kim, T. J. Shin and S. I. Seok, *Nature*, 2023, **616**, 724–730.
3 Z. Wang, Z. Song, Y. Yan, S. F. Liu and D. Yang, *Adv. Sci.*, 2019, **6**, 1801704.
4 K. Wang, L. Zheng, Y. Hou, A. Nozariasbmarz, B. Poudel, J. Yoon, T. Ye, D. Yang, A. V. Pogrebnyakov, V. Gopalan and S. Priya, *Joule*, 2022, **6**, 756–771.
5 K. O. Brinkmann, T. Becker, F. Zimmermann, C. Kreusel, T. Gahlmann, M. Theisen, T. Haeger, S. Olthof, C. Tuckmantel, M. Gunster, T. Maschwitz, F. Gobelsmann, C. Koch, D. Hertel, P. Caprioglio, F. Pena-Camargo, L. Perdigon-Toro, A. Al-Ashouri, L. Merten, A. Hinderhofer, L. Gomell, S. Zhang, F. Schreiber, S. Albrecht, K. Meerholz, D. Neher, M. Stolterfoht and T. Riedl, *Nature*, 2022, **604**, 280.
6 L. Tao, J. Qiu, B. Sun, X. Wang, X. Ran, L. Song, W. Shi, Q. Zhong, P. Li, H. Zhang, Y. Xia, P. Müller-Buschbaum and Y. Chen, *J. Energy Chem.*, 2021, **61**, 395–415.
7 S. Qin, C. Lu, Z. Jia, Y. Wang, S. Li, W. Lai, P. Shi, R. Wang, C. Zhu, J. Du, J. Zhang, L. Meng and Y. Li, *Adv. Mater.*, 2022, **34**, 2108829.
8 X. Meng, J. Wang, H. Wang, M. Li, D. Sun, X. Hu, J. He, P. Yu, J. Zhou, R. Chen, F. Ren, S. Liu, S. Zhang, Y. Zhang, Z. Zhao, Z. Liu and W. Chen, *Sol. RRL*, 2023, 2001557.
9 R. He, S. Q. Ren, C. Chen, Z. J. Yi, Y. Luo, H. G. Lai, W. W. Wang, G. G. Zeng, X. Hao, Y. Wang, J. Q. Zhang, C. L. Wang, L. L. Wu, F. Fu and D. W. Zhao, *Energy Environ. Sci.*, 2021, **14**, 5723–5759.
10 P. J. Hang, C. X. Kan, B. Li, Y. X. Yao, Z. C. Hu, Y. Q. Zhang, J. S. Xie, Y. Wang, D. R. Yang and X. G. Yu, *Adv. Funct. Mater.*, 2023, 2214381.
11 D. H. Kim, C. P. Muzzillo, J. Tong, A. F. Palmstrom, B. W. Larson, C. Choi, S. P. Harvey, S. Glynn, J. B. Whitaker, F. Zhang, Z. Li, H. Lu, M. F. A. M. van Hest, J. J. Berry, L. M. Mansfield, Y. Huang, Y. Yan and K. Zhu, *Joule*, 2019, **3**, 1734–1745.
12 Z. Li, J. Zhang, S. Wu, X. Deng, F. Li, D. Liu, C. C. Lee, F. Lin, D. Lei, C.-C. Chueh, Z. Zhu and A. K. Y. Jen, *Nano Energy*, 2020, **78**, 105377.
13 C. Chen, Z. Song, C. Xiao, R. A. Awni, C. Yao, N. Shrestha, C. Li, S. S. Bista, Y. Zhang, L. Chen, R. J. Ellingson, C. S. Jiang, M. Al-Jassim, G. Fang and Y. Yan, *ACS Energy Lett.*, 2020, **5**, 2560–2568.
14 J. Y. Ye, J. Tong, J. Hu, C. Xiao, H. Lu, S. P. Dunfield, D. H. Kim, X. Chen, B. W. Larson, J. Hao, K. Wang, Q. Zhao, Z. Chen, H. Hu, W. You, J. J. Berry, F. Zhang and K. Zhu, *Sol. RRL*, 2020, **4**, 2000082.
15 L. Wang, G. Wang, Z. Yan, J. Qiu, C. Jia, W. Zhang, C. Zhen, C. Xu, K. Tai, X. Jiang and S. Yang, *Sol. RRL*, 2020, **4**, 2000098.
16 K. Emshadi, N. Ghimire, A. Gurung, B. Bahrami, R. Pathak, R. S. Bobba, B. S. Lamsal, S. I. Rahman, A. H. Chowdhury, K. Chen, M. A. R. Laskar, W. Luo, H. Elbohy and Q. Qiao, *Sol. RRL*, 2020, **4**, 2000384.
17 S. Rothemund and I. Teasdale, *Chem. Soc. Rev.*, 2016, **45** 5200–5215.
18 J. Song, B. Zhang, J. Shi, J. Ma, G. Yang and B. Han, *Chin. J. Chem.*, 2012, **30**, 2079–2084.
19 C. Li, X. Wang, E. Bi, F. Jiang, S. M. Park, Y. Li, L. Chen, Z. Wang, L. Zeng, H. Chen, Y. Liu, C. R. Grice, A. Abudulimu, J. Chung, Y. Xian, T. Zhu, H. Lai, B. Chen, R. J. Ellingson, F. Fu, D. S. Ginger, Z. Song, E. H. Sargent and Y. Yan, *Science*, 2023, **379**, 690–694.
20 Z. Ma, R. Yu, Z. Xu, G. Wu, H. Gao, R. Wang, Y. Gong, J. Yang and Z. Tan, *Small*, 2022, **18**, 2201820.
21 J. Liang, X. Hu, C. Wang, C. Liang, C. Chen, M. Xiao, J. Li, C. Tao, G. Xing, R. Yu, W. Ke and G. Fang, *Joule*, 2022, **6**, 816–833.
22 X. Wang, L. Wang, T. Shan, S. Leng, H. Zhong, Q. Bao, Z. H. Lu, L. L. Deng and C. C. Chen, *Nano-Micro Lett.*, 2020, **12**, 84.
23 J. W. Xiang, J. H. Qi, Y. J. Cheng, K. Chen, Y. M. Ma, J. Y. Xie, Y. Hu, A. Y. Mei, Y. H. Zhou and H. W. Han, *Adv. Funct. Mater.*, 2023, 2300473.
24 L. Bi, Q. Fu, Z. Zeng, Y. Wang, F. R. Lin, Y. Cheng, H. L. Yip, S. W. Tsang and A. K. Jen, *J. Am. Chem. Soc.*, 2023, **145**, 5920–5929.
25 S. Ye, H. Rao, M. Feng, L. Xi, Z. Yen, D. H. L. Seng, Q. Xu, C. Boothroyd, B. Chen, Y. Guo, B. Wang, T. Salim, Q. Zhang, H. He, Y. Wang, X. Xiao, Y. M. Lam and T. C. Sum, *Nat. Energy*, 2023, **8**, 284–293.
26 W. Peng, K. Mao, F. Cai, H. Meng, Z. Zhu, T. Li, S. Yuan, Z. Xu, X. Feng, J. Xu, M. D. McGehee and J. Xu, *Science*, 2023, **379**, 683–690.
27 R. Wang, H. Gao, R. Yu, H. Jia, Z. Ma, Z. He, Y. Zhang, J. Yang, L. Zhang and Z. Tan, *J. Phys. Chem. Lett.*, 2021, **12**, 11772–11778.
28 X. Yang, Y. Chen, P. Liu, H. Xiang, W. Wang, R. Ran, W. Zhou and Z. Shao, *Adv. Funct. Mater.*, 2020, **30**, 2001557.

